REFERENCES

[1] H. Bai, M. Arcak, and J. Wen, *Cooperative Control Design: A Systematic, Passivity-Based Approach* (Communications and Control Engineering). New York, NY, USA: Springer-Verlag, 2011.

[2] S. P. Boyd, L. E. Ghaoui, E. Feron, and V. Balakrishnan, *Linear Matrix Inequalities in System and Control Theory*. Philadelphia, PA, USA: SIAM, 1994.

[3] F. Bullo, J. Cortes, and S. Martinez, *Distributed Control of Robotic Networks*. Princeton, NJ, USA: Princeton Univ. Press, 2009.

[4] Y. Cao and W. Ren, "Distributed coordinated tracking with reduced interaction via a variable structure approach," *IEEE Trans. Autom. Control*, vol. 57, no. 1, pp. 33–48, Jan. 2012.

[5] G. Chen and F. L. Lewis, "Distributed adaptive tracking control for synchronization of unknown networked Lagrangian systems," *IEEE Trans. Syst., Man Cybern. B, Cybern.*, vol. 41, no. 3, pp. 805–816, Jun. 2011.

[6] S.-J. Chung, U. Ahsun, and J.-J. E. Slotine, "Cooperative robot control and concurrent synchronization of Lagrangian systems," *IEEE Trans. Robot.*, vol. 25, no. 3, pp. 686–700, Jun. 2009.

[7] K. D. Do, "Flocking for multiple elliptical agents with limited communication ranges," *IEEE Trans. Robot.*, vol. 27, no. 5, pp. 931–942, Oct. 2011.

[8] W. Dong, "On consensus algorithms of multiple uncertain mechanical systems with a reference trajectory," *Automatica*, vol. 47, no. 9, pp. 2023–2028, 2011.

[9] N. Fischer, R. Kamalapurkar, and W. E. Dixon, "Lasalle-Yoshizawa corollaries for nonsmooth systems," *IEEE Trans. Autom. Control*, vol. 58, no. 9, pp. 2333–2338, Sep. 2013.

[10] R. Haghighi and C. C. Cheah, "Multi-group coordination control for robot swarms," *Automatica*, vol. 48, no. 10, pp. 2526–2534, 2012.

[11] P. F. Hokayem, D. M. Stipanovic, and M. W. Spong, "Semiautonomous control of multiple networked Lagrangian systems," *Int. J. Robust Nonlinear Control*, vol. 19, no. 18, pp. 2040–2055, 2009.

[12] J. Hu and Y. Hong, "Leader-following coordination of multi-agent systems with coupling time delays," *Physica A, Statist. Mech. Appl.*, vol. 374, no. 2, pp. 853–863, 2007.

[13] S. Khoo, L. Xie, and Z. Man, "Robust finite-time consensus tracking algorithm for multirobot systems," *IEEE/ASME Trans. Mechatronics*, vol. 14, no. 2, pp. 219–228, Apr. 2009.

[14] D. Lee and M. W. Spong, "Passive bilateral teleoperation with constant time delay," *IEEE Trans. Robot.*, vol. 22, no. 2, pp. 269–281, Apr. 2006.

[15] Y. Liu and N. Chopra, "Controlled synchronization of heterogeneous robotic manipulators in the task space," *IEEE Trans. Robot.*, vol. 28, no. 1, pp. 268–275, Feb. 2012.

[16] J. Mei, W. Ren, J. Chen, and G. Ma, "Distributed adaptive coordination for multiple Lagrangian systems under a directed graph without using neighbors' velocity information," *Automatica*, vol. 49, no. 6, pp. 1723–1731, 2013.

[17] J. Mei, W. Ren, and G. Ma, "Distributed coordinated tracking with a dynamic leader for multiple Euler-Lagrange systems," *IEEE Trans. Autom. Control*, vol. 56, no. 6, pp. 1415–1421, Jun. 2011.

[18] J. Mei, W. Ren, and G. Ma, "Distributed containment control for Lagrangian networks with parametric uncertainties under a directed graph," *Automatica*, vol. 48, no. 4, pp. 653–659, 2012.

[19] Z. Meng, Dimos V. Dimarogonas, and K. H. Johansson, "Zero-error coordinated tracking of multiple heterogeneous Lagrange systems using continuous control," in *Proc. 52nd Control Decis. Conf.*, Palazzo dei Congressi, Florence, Italy, 2013, pp. 2175–2180.

[20] Z. Meng, Z. Lin, and W. Ren, "Leader-follower swarm tracking for networked Lagrange systems," *Syst. Control Lett.*, vol. 61, no. 1, pp. 117–126, 2012.

[21] Z. Meng, W. Ren, Y. Cao, and Z. You, "Leaderless and leader-following consensus with communication and input delays under a directed network topology," *IEEE Trans. Syst., Man, Cybern. B, Cybern.*, vol. 41, no. 1, pp. 75–88, Feb. 2011.

[22] E. Nuno, R. Ortega, L. Basanez, and D. Hill, "Synchronization of networks of nonidentical Euler-Lagrange systems with uncertain parameters and communication delays," *IEEE Trans. Autom. Control*, vol. 56, no. 4, pp. 935–941, Apr. 2011.

[23] R. Olfati-Saber, J. A. Fax, and R. M. Murray, "Consensus and cooperation in networked multi-agent systems," *Proc. IEEE*, vol. 95, no. 1, pp. 215–233, Jan. 2007.

[24] B. E. Paden and S. S. Sastry, "A calculus for computing Filippov's differential inclusion with application to the variable structure control of robot manipulators," *IEEE Trans. Circuits Syst.*, vol. CAS-34, no. 1, pp. 73–82, Jan. 1987.

[25] W. Ren, "Distributed leaderless consensus algorithms for networked Euler-Lagrange systems," *Int. J. Control*, vol. 82, no. 11, pp. 2137–2149, 2009.

[26] D. Shevitz and B. E. Paden, "Lyapunov stability theory of nonsmooth systems," *IEEE Trans. Autom. Control*, vol. 39, no. 9, pp. 1910–1914, Sep. 1994.

[27] M. W. Spong, S. Hutchinson, and M. Vidyasagar, *Robot Dynamics and Control*. New York, NY, USA: Wiley, 2006.

[28] B. Xian, D. M. Dawson, M. S. de Queiroz, and J. Chen, "A continuous asymptotic tracking control strategy for uncertain nonlinear systems," *IEEE Trans. Autom. Control*, vol. 49, no. 7, pp. 1206–1211, Jul. 2004.

Stability Analysis of a Hierarchical Architecture for Discrete-Time Sensor-Based Control of Robotic Systems

Magnus Bjerkeng, Pietro Falco, Ciro Natale, and Kristin Y. Pettersen

***Abstract*—The stability of discrete time kinematic sensor-based control of robots is investigated in this paper. A hierarchical inner-loop/outer-loop control architecture common for a generic robotic system is considered. The inner loop is composed of a servo-level joint controller and higher level kinematic feedback is performed in the outer loop. Stability results derived in this paper are of interest in several applications including visual servoing problems, redundancy control, and coordination/synchronization problems. The stability of the overall system is investigated taking into account input/output delays and the inner loop dynamics. A necessary and sufficient condition that the gain of the outer feedback loop has to satisfy to ensure local stability is derived. Experiments on a Kuka K-R16 manipulator have been performed in order to validate the theoretical findings on a real robotic system and show their practical relevance.**

***Index Terms*—Calibration and identification, discrete-time stability, kinematics, output feedback control, redundant robots, velocity control.**

I. INTRODUCTION

Industrial robot manipulators have mainly been applied in highly tailored situations, where preprogrammed motions are sufficient for task completion. As the industry is looking to extend the use of manipulators to unstructured environments, pure motion control is no longer viable and sensor-based control must be introduced.

Feedback for motion control of robot manipulators in the control literature is usually considered in the continuous time framework, assuming direct torque input [1, Ch. 6]. These assumptions may hold for some model research platforms, whereas control interfaces of most

Manuscript received June 5, 2013; revised October 2, 2013; accepted December 9, 2013. Date of publication January 13, 2014; date of current version June 3, 2014. This paper was recommended for publication by Associate Editor Paolo Robuffo Giordano and Editor Giuseppe Oriolo upon evaluation of the reviewers' comments.This work was partly supported by the Italian Ministry of University and Scientific Research (PRIN 2009) under the national Project ROCOCO. This work is part of the research project Next Generation Robotics for Norwegian Industry. The project partners are The Research Council of Norway, SINTEF, NTNU, Statoil, Hydro, Tronrud Engineering, SbSeating, Glen Dimplex, Nordic and RobotNorge.

M. Bjerkeng is with the Department of Engineering Cybernetics, Norwegian University of Science and Technology, Trondheim NO-7491, Norway, and also with SINTEF ICT Applied Cybernetics, Trondheim NO-7034, Norway (e-mail: magnus.bjerkeng@sintef.no).

P. Falco and C. Natale are with the Dipartimento di Ingegneria Industriale 81031, e dell'Informazione, Seconda Università degli Studi di Napoli, Aversa, Italy (e-mail: pietro.falco@unina2.it; ciro.natale@unina2.it).

K. Y. Pettersen is with the Department of Engineering Cybernetics, Norwegian University of Science and Technology, Trondheim NO-7491, Norway (e-mail: Kristin.Y.Pettersen@itk.ntnu.no).

Color versions of one or more of the figures in this paper are available online at http://ieeexplore.ieee.org.

Digital Object Identifier 10.1109/TRO.2013.2294882

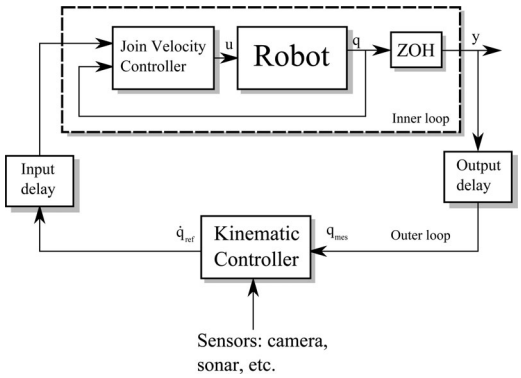

Fig. 1. Block diagram of a typical hierarchical motion control system.

industrial robots are greatly different [2]. In addition, even the users of the most advanced research robotic systems usually require access to the control interface at a level higher than the torque input since their algorithms are focused on higher levels of abstractions. Furthermore, for real systems, the control algorithms are always implemented in discrete time, and operational space motion control is often achieved using a hierarchical control architecture rather than through direct torque control [3].

A typical control hierarchy seen in robotics and marine crafts [4] is depicted in Fig. 1. The inner loop consists of a low-level velocity controller of some configuration coordinates, i.e., the joint servo loop in robotics. The outer loop calculates the desired joint velocities using a kinematic controller usually taking extrasensory information into account. Despite potentially lower performance, a hierarchical control design has advantages over centralized torque controllers with respect to modularity, portability, safety, and computational cost [5].

Since it is typically not possible for the user to tune or alter the inner servo loops, the control design is deferred to performing kinematic feedback in the outer loop. A much used kinematic control law is the *resolved motion rate controller* (RMRC) first proposed in [6]. This controller is the pseudoinverse variant of the *closed-loop inverse-kinematics* (CLIK) class of controllers [7].

The practice of using the outer loop RMRC to achieve operational space motions is well established, and some popular applications include visual servoing [8], redundancy resolution (typically with respect to obstacle avoidance or manipulability) [9], multirobot coordination [10], velocity-field control [11], effective task sequencing [12], robotic and human manipulation [13]. Note that this list is in no way exhaustive.

Most commonly in implementation, the RMRC method is used as a trajectory generator, only using actual state measurements initializing the controllers state [9]. However, as interaction with unstructured environments is becoming an increasingly relevant robotic application, additional sensors have to be introduced. Such sensors are typically cameras, e.g., the Microsoft Kinect sensor, or force/torque sensors. For static or slowly moving environments, sensory signals will still be predominantly dependent on the robots configuration, such that they can be considered as configuration dependent functions in the RMRC formulation. The use of output feedback with trajectory generation is sometimes simply called trajectory generation, while [14] suggests the term online trajectory generation to specify that sensory feedback is used.

Surprisingly, given the popularity of the RMRC, the stability properties pertaining to the output-feedback case has not been the focus of much research. Several stability results exist for trajectory generation, which do not consider system dynamics and delays, and are hence not valid when sensors are used in the feedback loop. This is the main motivation for performing a more detailed analysis of the full-system stability properties, which arise when using feedback from external sensors with the RMRC.

Stability results for the continuous-time case without delays have previously appeared in the literature. The first stability study is found in [15], where Lyapunov analysis is used to show uniform ultimate boundedness with a computed-torque type controller in the inner loop. A systematic design procedure, which takes into account the inner-loop dynamics, has been presented in [16] but for the specific case of force control. Global exponential stability is reported in [17] for the continuous-time case using cascade theory, again with a computed-torque type inner loop. Most recently, uniform ultimate boundedness is shown using a PI-controller in the inner loop [18].

However, for the discrete-time case, results only exist for very simplified systems, i.e., without considering inner-loop dynamics or time delays. The motivation behind these assumptions is that the RMRC is used for open-loop trajectory generation rather than for feedback control. The latest result regarding the stability of the RMRC for trajectory generation is found in [19], where input bounds, which are sufficient for local exponential stability of the equilibrium as well as a tight estimate of the region of attraction, are derived.

In this paper, we extend the results obtained in [19] about the stability of RMRC in the discrete-time framework by taking dynamics of the inner loop into account and including input–output delays. The introduction of these nonideal effects will give results, which better represent the reality faced when dealing with control of robots with a discrete-time control interface. The presented stability results are not only desirable for the completeness of the literature, but also for determining how the inner-loop dynamics affects the overall stability of the closed-loop system, especially with respect to feedback gains.

The contributions in this paper are as follows. A discrete-time linear input/output dynamical model is proposed to describe the robot motion under velocity servo control. Input/output data from a real industrial manipulator are used to verify the model. The local stability of the RMRC for the inner-loop/outer-loop velocity control architecture subject to delays, where the inner loop is assumed to have stable linear velocity dynamics, is determined. The derivation of outer-loop gain margins is then presented in a closed form for small delays. For arbitrarily high delays, a small-gain condition is derived for the outer loop feedback gain, and a numerical method is proposed for the limit gain computation.

This paper is organized in the following way. In Section II, the robot model is introduced along with adopted notation. The specific problem statement is stated in Section III, which recalls some results of [19]. The error dynamics is derived in Section IV, followed by a Lyapunov-based stability proof in Section V. Quantitative conditions that the feedback gains should satisfy in order to guarantee closed-loop stability are derived in Section VI. Experimental validation of the theoretical findings is presented in Section VII. Conclusions and further work are found in Section VIII.

II. Robot Model

In this section, we introduce the robot's dynamical model and the notation used in this paper. Please note that the robot dynamics introduced now is the discrete-time input–output dynamics of the robot under servo control, i.e., the dashed box in Fig. 1. The reference velocity in the configuration space is the input and the actual position is the output. We propose a linear model for these dynamics, which will

be the case if for instance feedback linearization or computed torque is used in the inner loop [15].

Consider a robotic system with configuration variables $\boldsymbol{q} \in \mathbb{R}^n$. The position at time $k \in \mathbb{Z}^+$ is given by $\boldsymbol{q}_k$. The sampling period is T, and the continuous time is given by $t = Tk$. A reference velocity $\dot{\boldsymbol{q}}_k^{\text{ref}}$ is passed to the robot controller at time k. The inner-loop dynamics of each joint are assumed decoupled, with identical convergence rates for each joint. The assumption that all joint have the same convergence rate a is a homogeneity assumption, as opposed to the heterogeneous case, where a_i are not all identical. Denoting the convergence rate by $a \in (-1, 1)$, the input gain as $b > 0$, and the input time delay by d_I results in the following robot model for the joint increment $\Delta \boldsymbol{q}_k = \boldsymbol{q}_k - \boldsymbol{q}_{k-1:}$

$$\Delta \boldsymbol{q}_{k+1} = a \Delta \boldsymbol{q}_k + bT \dot{\boldsymbol{q}}_{k-d_I}^{\text{ref}}. \tag{1}$$

Here, $a = 0$ corresponds to a perfect velocity controller, which converges in one step, a close to 1 corresponds to a slow "overdamped" joint dynamics, and a close to -1 results in a slowly converging "underdamped" dynamics with oscillations. The input parameter b is expected to fulfill $b \approx 1$ for a well-behaved system, such that a commanded velocity is achieved with a small error. Experiments that show how well the proposed model describes the velocity dynamics of an industrial manipulator are reported in Section VII-A.

III. Problem statement

In this section, the problem statement is presented, and we recall the RMRC for set-point regulation.

Let $\boldsymbol{e} \in \mathcal{E}$ be the vector of task error variables of a robotic system, with $\mathcal{E}$ being a domain of $\mathbb{R}^m$, and let $\boldsymbol{q} \in \mathcal{Q}$ be the vector of the robotic system configuration variables, with $\mathcal{Q}$ being a domain of $\mathbb{R}^n$ with $m \leq n$, such that

$$\boldsymbol{e}(\boldsymbol{q}) : \mathcal{Q} \subseteq \mathbb{R}^n \mapsto \mathcal{E} \subseteq \mathbb{R}^m. \tag{2}$$

For example, in a robotic manipulator, $\boldsymbol{e}(\boldsymbol{q})$ may be the position error of the end effector, and $\boldsymbol{q}$ is the vector of joint positions, whereas in a platoon of mobile robots, $\boldsymbol{q}$ is the vector of coordinates representing the location of each robot, and $\boldsymbol{e}(\boldsymbol{q})$ is the vector of suitable task errors, depending on the mission, e.g., move the centroid of the formation to a desired location.

The robot is said to be executing its task if $\boldsymbol{e} = \boldsymbol{0}$. The task Jacobian is defined as $\mathbf{J}(\boldsymbol{q}) = \frac{\partial \boldsymbol{e}}{\partial \boldsymbol{q}} \in \mathbb{R}^{m \times n}$. For a *task redundant* problem, we have $m < n$ using the definition in [20]. More precisely the control objective may be stated as follows.

Determine if there exist a positive feedback gain k_p, and admissible initial conditions $\boldsymbol{q}_0, \Delta \boldsymbol{q}_0$, such that (1) in conjunction with

$$\dot{\boldsymbol{q}}_k^{\text{ref}} = -k_p \mathbf{J}^{\dagger}(\boldsymbol{q}_{k-d_O}) \boldsymbol{e}(\boldsymbol{q}_{k-d_O}) \tag{3}$$

implies that

$$\lim_{k \to \infty} \|\boldsymbol{e}_k\| = 0. \tag{4}$$

In the control law (3), $d_O \in \mathbb{Z}^+$ is the output delay, and $\boldsymbol{q}_{k-d_O}$ are the delayed measurements of the configuration variables. In other words, determine if the RMRC (3) in a closed loop with the robot dynamics (1) will have $\boldsymbol{e} = 0$ as a stable equilibrium point.

A. Assumptions

In this section, we state the assumptions that the results in this paper will be based on. These assumptions are the same as considered in [19] and are necessary for a well-posed problem in terms of existence of solutions to (1) and (3).

1) $\exists\ \delta \in \mathbb{R}^+ : \|\mathbf{J}(\boldsymbol{q})\| < \delta \quad \forall\, \boldsymbol{q} \in \mathcal{Q}$.
2) $\exists\ \beta \in \mathbb{R}^+ : \underline{\sigma}(\mathbf{J}\mathbf{J}^T) \geq \beta \quad \forall\, \boldsymbol{q} \in \mathcal{Q}$.
3) $\exists\ \zeta \in \mathbb{R}^+ : \|\frac{\partial^2 e_i(\boldsymbol{q})}{\partial \boldsymbol{q}^2}\| \leq \zeta \quad \forall\, \boldsymbol{q} \in \mathcal{Q},\ i \in [1, n]$.

Here, as the matrix norm, the spectral norm, i.e., the largest singular value, has been assumed, and the symbol $\underline{\sigma}(\mathbf{X})$ denotes the smallest singular value of the matrix $\mathbf{X}$. Assumptions 1 and 3 impose smoothness constraints on the task description, as they assume that the norms of both the Jacobian and Hessian of $\boldsymbol{e}$ are bounded on $\mathcal{Q}$. These smoothness assumptions hold for example for the direct kinematics of revolute-joint manipulators. Assumption 2 specifies that the Jacobian has full rank, and is some *distance* away from a singularity. It is assumed that the configuration $\boldsymbol{q}$ stays in $\mathcal{Q}$ for all time.

B. Preliminaries

In this section, the error dynamics of the proposed system (1) and (3) is derived. To this end, Taylor's theorem with explicit second-order Lagrange remainders is used. We shortly recall the Lagrange remainder result, which is similar to our approach, used in [19] to determine the linearized error-dynamics. The Taylor expansion of $\boldsymbol{e}(\boldsymbol{q} + \boldsymbol{\epsilon})$ around $\boldsymbol{q}$ for some $\boldsymbol{\epsilon} \in \mathbb{R}^n$ is given by

$$\boldsymbol{e}(\boldsymbol{q} + \boldsymbol{\epsilon}) = \boldsymbol{e}(\boldsymbol{q}) + \mathbf{J}(\boldsymbol{q})\boldsymbol{\epsilon} + \boldsymbol{r}(\boldsymbol{q}, \boldsymbol{\epsilon}, \boldsymbol{\zeta}) \tag{5}$$

where the Lagrange remainder $\boldsymbol{r}$ is given by

$$\boldsymbol{r}(\boldsymbol{q}, \boldsymbol{\epsilon}, \boldsymbol{\zeta}) = \frac{1}{2} \begin{bmatrix} \boldsymbol{\epsilon}^T \left.\dfrac{\partial^2 e_1(\boldsymbol{q})}{\partial \boldsymbol{q}^2}\right|_{\boldsymbol{q} + \zeta_1 \boldsymbol{\epsilon}} \boldsymbol{\epsilon} \\ \vdots \\ \boldsymbol{\epsilon}^T \left.\dfrac{\partial^2 e_m(\boldsymbol{q})}{\partial \boldsymbol{q}^2}\right|_{\boldsymbol{q} + \zeta_m \boldsymbol{\epsilon}} \boldsymbol{\epsilon} \end{bmatrix} \tag{6}$$

for some $\boldsymbol{\zeta} \in \mathbb{R}^n$ where all the elements of $\boldsymbol{\zeta}$ belong to the range $[0, 1]$. Note that, as shown by [19, Lemma 1], assumption 3 implies that $\boldsymbol{r}$ in (5) is bounded such that

$$\|\boldsymbol{r}\| \leq \nu \|\boldsymbol{\epsilon}\|^2 \tag{7}$$

for some $\nu \in \mathbb{R}^+$.

The discrete-time variant of the Lyapunov's second method for determining the stability of fixed points will also be used. Please see [21] for a detailed presentation of this.

The stability proof found here and the previous proof found in [19] are quite different. In the open-loop case previously considered, it was possible to derive time-invariant dynamics using the norm of the task error as a scalar state. This was not possible for the output-feedback case considered here and Lyapunov analysis is used instead. The assumptions used are identical in both paper, as well as the use of Lagrange remainders.

IV. Error dynamics analysis

In this section, a linearization of the task-error dynamics is developed. The input/output delays are lumped as $d = d_I + d_O$, and we consider the following state vector

$$\boldsymbol{z}_k = \begin{bmatrix} \boldsymbol{e}_{k-d} \\ \vdots \\ \boldsymbol{e}_k \\ \Delta \boldsymbol{q}_{k-d} \\ \vdots \\ \Delta \boldsymbol{q}_k \end{bmatrix} = \begin{bmatrix} \boldsymbol{z}_{e_k} \\ \boldsymbol{z}_{q_k} \end{bmatrix}. \tag{8}$$

Note that the increments of configuration variables $\boldsymbol{z}_q$ are included in the state $\boldsymbol{z}$, since only the convergence to zero of the task-space error $\boldsymbol{e}_k$ is not enough to prove the stability of the algorithm. For redundant tasks, $\boldsymbol{e}_k = \boldsymbol{0}$ does not directly imply that $\Delta\boldsymbol{q}_{k+1} = \boldsymbol{0}$, i.e., the absence of internal motions is not guaranteed even if the error dynamic is stable. By also including the configuration increment in the state, it is possible to verify that the increment $\Delta\boldsymbol{q}_k$ tends to zero.

The proof presented in the next section is a linearization type proof. The goal of this section is hence to derive the dynamics for the state (8) such that the main stabilizing effects of the system appears linearly in the error dynamics. We will in our analysis group higher order terms which satisfy

$$\|\boldsymbol{r}\| \leq \alpha\|\boldsymbol{z}\|^p, \quad p \geq 2, \alpha > 0 \tag{9}$$

denoting them collectively as $\boldsymbol{r}$ for brevity.

The Taylor series of vector-valued functions is the main tool used in the linearization procedure, and the expansions of the task function may be written as

$$\boldsymbol{e}_{k+1} = \boldsymbol{e}(\boldsymbol{q}_k + \Delta\boldsymbol{q}_{k+1}) = \boldsymbol{e}_k + \mathbf{J}_k\Delta\boldsymbol{q}_{k+1} + \boldsymbol{r} \tag{10}$$

where $\|\boldsymbol{r}\| \leq \nu\|\boldsymbol{z}_k\|^2$ by Assumption 3.

Substituting the controller equation (3) into (1) describing the dynamics of $\Delta\boldsymbol{q}_k$, we have

$$\Delta\boldsymbol{q}_{k+1} = a\Delta\boldsymbol{q}_k - k_p bT\mathbf{J}^{\dagger}_{k-d}\boldsymbol{e}_{k-d}. \tag{11}$$

Therefore, in view of Assumption 3, (7), (10), and standard norm properties, the remainder $\boldsymbol{r}$ is bounded as

$$\|\boldsymbol{r}\| \leq \nu\|\Delta\boldsymbol{q}_{k+1}\|^2 \leq \nu\left(a\|\Delta\boldsymbol{q}_k\| + k_p T|b|\|\mathbf{J}^{\dagger}_{k-d}\|\|\boldsymbol{e}_{k-d}\|\right)^2.$$

Using Assumptions 1 and 2, the Jacobian pseudoinverse can be bounded as

$$\|\mathbf{J}^{\dagger}(\boldsymbol{q}_{k-d})\| \leq \frac{\delta}{\beta} = \eta \quad \forall\boldsymbol{q} \in \mathcal{Q} \tag{12}$$

hence

$$\|\boldsymbol{r}\| \leq \nu_1^2\|\Delta\boldsymbol{q}_k\|^2 + \nu_2^2\|\boldsymbol{e}_{k-d}\|^2 + 2\nu_1\nu_2\|\Delta\boldsymbol{q}_k\|\|\boldsymbol{e}_{k-d}\| \leq \bar{\nu}\|\boldsymbol{z}_k\|^2$$

where the positive constants ν_1, ν_2, and $\bar{\nu}$ are suitably defined. To resolve the configuration dependent term $\mathbf{J}_k\Delta\boldsymbol{q}_k$, appearing after the substitution of (11) in (10), the Taylor series of $\boldsymbol{e}_{k-1}$ is evaluated as follows:

$$\boldsymbol{e}(\boldsymbol{q}_{k-1}) = \boldsymbol{e}(\boldsymbol{q}_k - \Delta\boldsymbol{q}_k) \tag{13}$$

$$\boldsymbol{e}_{k-1} = \boldsymbol{e}_k - \mathbf{J}_k\Delta\boldsymbol{q}_k + \boldsymbol{r}. \tag{14}$$

Here, the reminder $\boldsymbol{r}$ is bounded by $\|\Delta\boldsymbol{q}_k\|^2$ and thus by $\|\boldsymbol{z}_k\|^2$. Solving (14) for the first-order term gives the following expression:

$$\mathbf{J}_k\Delta\boldsymbol{q}_k = \boldsymbol{e}_k - \boldsymbol{e}_{k-1} + \boldsymbol{r} \tag{15}$$

then (10) becomes

$$\boldsymbol{e}_{k+1} = (1+a)\boldsymbol{e}_k - a\boldsymbol{e}_{k-1} - k_p bT\mathbf{J}_k\mathbf{J}^{\dagger}_{k-d}\boldsymbol{e}_{k-d} + \boldsymbol{r} \tag{16}$$

where all the reminders are lumped in $\boldsymbol{r}$. To resolve the last indeterminate term, we evaluate $\mathbf{J}_k\mathbf{J}^{\dagger}_{k-d}\boldsymbol{e}_{k-d}$ using the Talyor expansion of the task Jacobian

$$\mathbf{J}_k = \mathbf{J}(\boldsymbol{q}_{k-1} + \Delta\boldsymbol{q}_k) = \mathbf{J}_{k-1} + \mathbf{R}_1(\Delta\boldsymbol{q}_k) \tag{17}$$

where $\mathbf{R}_1$ is a matrix which satisfies $\|\mathbf{R}_1(\Delta\boldsymbol{q}_k)\| \leq \nu_3\|\Delta\boldsymbol{q}_k\|$ using Assumption 3. The matrix $\mathbf{R}_1$ may be calculated by considering the Taylor expansions of the columns of $\mathbf{J}(\boldsymbol{q}_{k-1} + \Delta\boldsymbol{q}_k)$ around $\boldsymbol{q}_{k-1}$, and evaluating the second-order Lagrange reminder explicitly as in (5). Applying (17) iteratively gives

$$\mathbf{J}_k = \mathbf{J}_{k-d} + \mathbf{R}_1(\Delta\boldsymbol{q}_k) + \ldots + \mathbf{R}_d(\Delta\boldsymbol{q}_{k-d+1}). \tag{18}$$

The linearization of (10) is completed by inserting (18) into (16) and collecting the reminders noting that $\mathbf{R}_i\boldsymbol{e}_{k-d}$, $i = 1, \ldots, d$ are all bounded by $\|\boldsymbol{z}_k\|^2$ such that

$$\boldsymbol{e}_{k+1} = (1+a)\boldsymbol{e}_k - a\boldsymbol{e}_{k-1} - k_p Tb\boldsymbol{e}_{k-d} + \boldsymbol{r}(\boldsymbol{z}_k). \tag{19}$$

In (19), Assumption 2 is used to equate $\mathbf{J}_{k-d}\mathbf{J}^{\dagger}_{k-d} = \mathbf{I}_m$, where the $\mathbf{I}_m$ denotes the $m \times m$ identity matrix.

We will shortly comment on some noteworthy features of the linearized task-error dynamics (19). It is seen that the linear part of (19) is identical to the configuration-space dynamics (1) under proportional set-point control, $\dot{\boldsymbol{q}}_{\mathrm{ref}} = -k_p(\boldsymbol{q} - \boldsymbol{q}_{\mathrm{ref}})$. This is analogous to the continuous-time case [9], disregarding the disturbance term. The nonlinear disturbance term $\boldsymbol{r}(\boldsymbol{z}_k)$, which is perturbing the error dynamics, is a function of current and delayed error signals as well as position increments. This coupling of the zero dynamics does not allow a distributed analysis such as the cascade analysis done in [17].

V. Stability analysis

In this section, the stability property of the error dynamics derived in the previous section is determined. We will use Lyapunov's second method for discrete-time systems [21], with a quadratic Lyapunov function candidate.[1] The error dynamics previously derived has the following state-space realization

$$\boldsymbol{z}_{k+1} = \begin{bmatrix} \boldsymbol{z}_{e_{k+1}} \\ \boldsymbol{z}_{q_{k+1}} \end{bmatrix} = \begin{bmatrix} \mathbf{A}_{ee} & \mathbf{0} \\ \mathbf{A}_{qe}(\boldsymbol{q}_{k-d}) & \mathbf{A}_{qq} \end{bmatrix} \begin{bmatrix} \boldsymbol{z}_{e_k} \\ \boldsymbol{z}_{q_k} \end{bmatrix} + \boldsymbol{r}(\boldsymbol{z}_k) \tag{20}$$

where

$$\mathbf{A}_{ee} = \begin{bmatrix} \mathbf{0}_{dm\times m} & \mathbf{I}_{dm} \\ -Tbk_p\mathbf{I}_m & \mathbf{A}_s \end{bmatrix} \tag{21}$$

$$\mathbf{A}_s = [\,\mathbf{0}_m \quad \ldots \quad -a\mathbf{I}_m \quad (a+1)\mathbf{I}_m\,] \tag{22}$$

$$\mathbf{A}_{qq} = \begin{bmatrix} \mathbf{0}_{dn\times n} & \mathbf{I}_{dn} \\ \mathbf{0}_{n\times dn} & a\mathbf{I}_n \end{bmatrix} \tag{23}$$

$$\mathbf{A}_{qe_k} = [\,\mathbf{J}^{\dagger}(\boldsymbol{q}_{k-d}) \quad \mathbf{0}_{(d+1)n\times dm}\,]. \tag{24}$$

Due to the terms $\mathbf{A}_{qe}(\boldsymbol{q}_{k-d})$ and $\boldsymbol{r}(\boldsymbol{z}_k)$, system (20) is a nonlinear difference equation. For the stability analysis, we note that $\mathbf{A}_{qq}$ is a Schur matrix with eigenvalues at 0 and a. The analysis of the eigenvalues of $\mathbf{A}_{ee}$ is more involved, and is summarized in the following small-gain condition.

Proposition 1: There exist for any delay d a feedback gain $k_p > 0$ small enough such that $\mathbf{A}_{ee}$ is a Schur matrix. Proof: See the Appendix.

For the stability analysis it is necessary to use Lyapunov theory since the full error dynamics is nonlinear and configuration varying. The configuration dependence is considered as a time dependence in the remainder of the proof. For completeness, we recall the discrete-time definition of a Lyapunov function and the discrete-time equivalent to the LaSalle–Krasovsky Theorem.

Definition 1: Lyapunov Function [21]. *Consider the discrete-time system*

$$\boldsymbol{z}_{k+1} = \boldsymbol{f}(k, \boldsymbol{z}_k). \tag{25}$$

[1] An application originally considered by Hurt in [21] was the stability of the Newton–Raphson method, which is a special case of our system assuming no dynamics in the inner loop, no delays, and a nonredundant task description.

Let $\mathcal{G}$ be a set in the vector space $\boldsymbol{X}$. Let $V(k, \boldsymbol{z}_k), W(\boldsymbol{z}_k)$ be real-valued functions defined for all $k > k_0$ and for all $\boldsymbol{z}$ in $\mathcal{G}$. If $V(k, \boldsymbol{z}_k)$ and $W(\boldsymbol{z}_k)$ are continuous in z and $V(k, \boldsymbol{z}_k)$ is bounded from below, and

$$\Delta V_{k+1} = V(k+1, \boldsymbol{z}_{k+1}) - V(k, \boldsymbol{z}_k) \leq W(\boldsymbol{z}_k) \leq 0 \tag{26}$$

for all $k > k_0$ and for all $\boldsymbol{z} \in \mathcal{G}$, then V is called a Lyapunov function for the system (25) on $\mathcal{G}$.

LaSalle-Krasovsky Theorem [21]*: Let $\bar{\mathcal{G}} = \mathcal{G} \cup \{\infty\}$ be the closure of $\mathcal{G}$ including ∞ if $\mathcal{G}$ is unbounded. If there exists a Lyapunov function V for (25) on $\mathcal{G}$ and each solution of (25) remain in $\mathcal{G}$ for all $k > k_0$, then the set*

$$\mathcal{A} = \{\boldsymbol{z} \in \bar{\mathcal{G}} : W(\boldsymbol{z}) = 0\} \cup \{\infty\} \tag{27}$$

is uniformly asymptotically stable.

Consider the following quadratic Lyapunov function candidate:

$$V(\boldsymbol{z}_k) = \boldsymbol{z}_{e_k}^T \mathbf{P}_e \boldsymbol{z}_{e_k} + \boldsymbol{z}_{q_k}^T \mathbf{P}_q \boldsymbol{z}_{q_k} \tag{28}$$

where $\mathbf{P}_e, \mathbf{P}_q$ solves the discrete time Lyapunov equations for $\mathbf{A}_{ee}$ and $\mathbf{A}_{qq}$, respectively. The existence of the matrices $\mathbf{P}_e, \mathbf{P}_q$ are ensured by the linear discrete-time Lyapunov theorem (see [21]). Note that the positive definiteness of $\mathbf{P}_e$ and $\mathbf{P}_q$ ensures that V is bounded from above and below by quadratic functions of the state. The matrix $\mathbf{P}_q$ is for simplicity normalized such that $\|\mathbf{P}_q\| = 1$. We will show local asymptotic stability by demonstrating that $\Delta V_{k+1} = V_{k+1} - V_k < 0$ close to $\boldsymbol{z}_k = 0$. We will throughout the analysis disregard the superquadratic terms as they vanish sufficiently close to the origin. Inserting $\boldsymbol{z}_{k+1}$ into ΔV_{k+1} gives the following quadratic terms:

$$\begin{aligned}\Delta V_{k+1} = \boldsymbol{z}_{e_k}^T (\underbrace{\mathbf{A}_{ee}^T \mathbf{P}_e \mathbf{A}_{ee} - \mathbf{P}_e}_{-\beta_e \mathbf{I}} + \mathbf{A}_{qe_k}^T \mathbf{P}_q \mathbf{A}_{qe_k}) \boldsymbol{z}_{e_k} + \dots \\ \times \boldsymbol{z}_{q_k}^T (\underbrace{\mathbf{A}_{qq}^T \mathbf{P}_q \mathbf{A}_{qq} - \mathbf{P}_q}_{-\beta_q \mathbf{I}}) \boldsymbol{z}_{q_k} + 2 \boldsymbol{z}_{q_k}^T \boldsymbol{A}_{qq}^T \mathbf{P}_q \mathbf{A}_{qe_k} \boldsymbol{z}_{e_k}\end{aligned} \tag{29}$$

where β_e and β_q are positive constants given by the discrete time Lyapunov equations for $\mathbf{A}_{ee}$ and $\mathbf{A}_{qq}$. Using (12) and (24), the time varying term is bounded as

$$\|\mathbf{A}_{qe_k}\| = \eta \quad \forall k \geq 0. \tag{30}$$

The following bounds are calculated directly from the definition of the matrices

$$\|\mathbf{A}_{qq}\| = \sqrt{a^2 + 1} = \nu, \quad \|\mathbf{P}_q\| = 1 \tag{31}$$

such that

$$\Delta V_{k+1} \leq (\eta^2 - \beta_e)\|\boldsymbol{z}_{e_k}\|^2 - \beta_q \|\boldsymbol{z}_{q_k}\|^2 + 2\nu\eta \|\boldsymbol{z}_{q_k}\| \|\boldsymbol{z}_{e_k}\|.$$

The cross term can be handled using Young's inequality

$$2\|\boldsymbol{z}_{q_k}\| \|\boldsymbol{z}_{e_k}\| \leq \frac{\|\boldsymbol{z}_{e_k}\|^2}{\epsilon} + \epsilon \|\boldsymbol{z}_{q_k}\|^2 \tag{32}$$

which gives an upper bound on ΔV_{k+1} in the following quadratic form:

$$\Delta V_{k+1} \leq \left(\frac{\nu\eta}{\epsilon} + \eta^2 - \beta_e\right) \|\boldsymbol{z}_{e_k}\|^2 + (\nu\eta\epsilon - \beta_q)\|\boldsymbol{z}_{q_k}\|^2.$$

We can choose the control analysis parameters such that the quadratic terms are negative. In particular, with the choice $\beta_e > \frac{\nu\eta}{\epsilon} + \eta^2$ and $\epsilon < \frac{\beta_q}{\eta\nu}$, we have

$$\Delta V_{k+1}(\boldsymbol{z}_k) \leq -\beta_z \|\boldsymbol{z}_k\|^2 + r(\|\boldsymbol{z}_k\|) = W(\boldsymbol{z}_k) \tag{33}$$

for some constant $\beta_z > 0$. Recall that the terms of order 3 or higher are lumped in $r(\|\boldsymbol{z}_k\|)$.

By defining a set around the origin for which ΔV is negative

$$\mathcal{G}(z^*) = \{\boldsymbol{z} : \|\boldsymbol{z}\| < z^* \Rightarrow \Delta V \leq 0\} \tag{34}$$

it is apparent by *Definition 1* that function (28) is a Lyapunov function for system (20) on $\mathcal{G}$. Note that it is not necessary to consider the closure of $\mathcal{G}$ with infinity since $\mathcal{G}$ is bounded.

In order to show asymptotic stability using *Theorem 1*, we need to show that $\boldsymbol{z}_k$ stays in $\mathcal{G}$ for all time, then $\boldsymbol{z}_k$ tends to the set $-\beta_z \|\boldsymbol{z}_k\|^2 + r(\|\boldsymbol{z}_k\|) = 0$ on $\mathcal{G}$. This is the origin as $-\beta_z \|\boldsymbol{z}_k\|^2 + r(\|\boldsymbol{z}_k\|)$ is negative on $\mathcal{G}$ by construction, except for $\boldsymbol{z}_k = \mathbf{0}$.

To ensure that solutions stay in $\mathcal{G}$ for all time, we need to construct a positive invariant set around the origin. Corollary 2 from [21] allows us to construct such a set using the upper and lower quadratic bounds on V, implying that sufficiently small initial conditions stay in $\mathcal{G}$ for all time. The existence of these bounds are given since the chosen Lyapunov function is quadratic. This establishes the uniform (in $\boldsymbol{q}_k$) asymptotic stability of the origin for (20). The result of the proof is summarized in the following.

Theorem 2: If k_p is chosen small enough such that Proposition 1 holds, then $\boldsymbol{e} = \mathbf{0}$ is a locally uniformly *(in $\boldsymbol{q}_k$)asymptotically stable equilibrium point for the system (1) in a closed loop with the controller (3).*

The stability of $\boldsymbol{e} = \mathbf{0}$ under the nonlinear feedback (3) is hence the same as for a linear output-feedback which is intuitively what one might expect. During implementation, one is typically also interested in the maximal feedback gain, which is considered in the following section.

VI. Feedback Gain Threshold

In this section, the maximum feedback gain $k_{p_{\max}}$ is analyzed. The maximum feedback gain is interesting for tuning purposes, and also for comparison with previous results from the literature. First, we will consider the delay-free case, i.e., when $d = 0$. In this case, the characteristic polynomial of A_{ee}, reported in the Appendix as Eq. (45), is

$$\left(\lambda^2 + (k_p T b - (a+1))\lambda + a\right)^m \tag{35}$$

and thus, by applying Jury's stability criterion, the limit gain k_p as a function of the system parameters is determined as

$$k_p < \frac{(1+a)}{b} \frac{2}{T}. \tag{36}$$

A non-minimum phase inner loop with $a = -1 + \epsilon$ for $0 < \epsilon \ll 1$ is the worst case in terms of gain margins, with an upper bound of the order of $\frac{2\epsilon}{bT}$. It is also observed that a less accurate velocity controller, for small b, implies that a higher gain is possible while maintaining stability. Previous results assume that $a = 0, b = 1$, which means perfect inner-loop control or trajectory generation. In this case, the upper gain margin is $k_p < \frac{2}{T}$, which is identical to the one derived by [19]. The result (36) presented here is thus a generalization of the results in [19].

For the case with $d = 1$, by resorting to (45) and to Jury criterion, the input gain $k_p < (1-a)/Tb$ is obtained. For larger delay, $d > 1$, we calculate k_p numerically.

In view of the expression of the characteristic polynomial of A_{ee} in (45), this can be done for example, by drawing the root locus of the transfer function

$$\frac{Tb}{\lambda^{d+1} - (1+a)\lambda^d + a\lambda^{d-1}}. \tag{37}$$

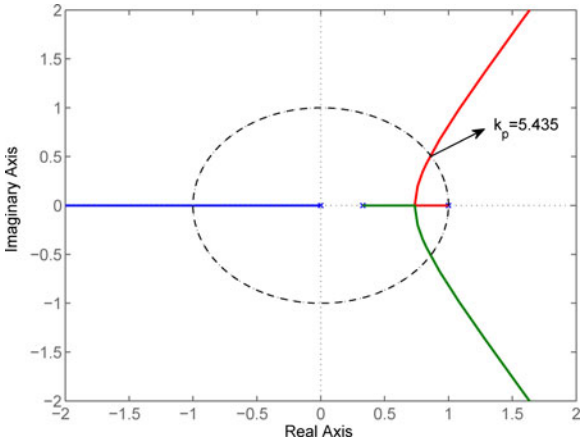

Fig. 2. Root locus of 37 with $d = 2$, $a = 0.329$, $b = 0.975$, and $T = 75$ ms.

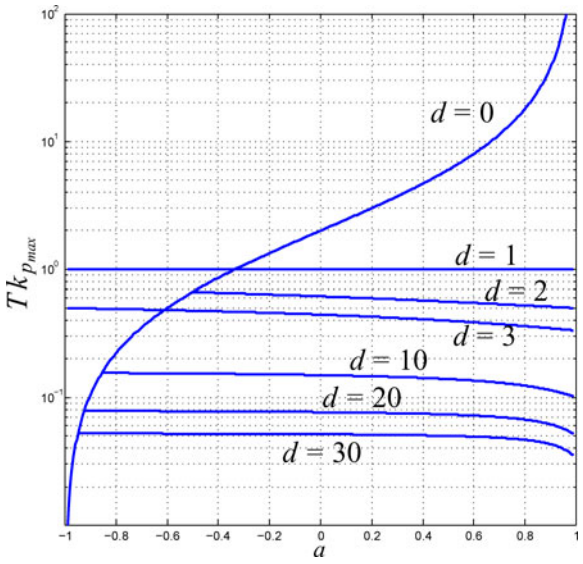

Fig. 3. Limit values of $k_p T$ as a function of the parameter a for different delays assuming that $b = (1 - a)$.

Fig. 2 shows the root locus in the case $d = 2$, $a = 0.329$, and $b = 0.975$, i.e., the values considered in the experiments (see Section VII). The maximum value of the gain can be easily determined as the minimum among the values corresponding to the intersections between the root locus and the unit circle. It this case, we have a limit gain $k_p = 0.4076/T = 5.435$. This limit gain decreases as d increases since the number of branches going outside the unit circle also increases.

A plot of numerically computed threshold feedback gains for different delays is seen in Fig. 3. It is in the calculation assumed that $b = (1 - a)$, which implies an exponentially converging velocity response for a constant velocity reference. It is seen that the maximum gain decreases with higher delays, and that the input bound (36) seems to hold for small a. Note that decreasing the sampling time T will in all these cases allow for a higher feedback gain in the outer loop. A brief consideration is due about the robustness. Since a small gain result has been derived, it is always possible to find a gain small enough such that the algorithm is stable. For example, a way to guarantee robustness to parameters uncertainties is to set the gain considering the worst-case estimation of the parameters.

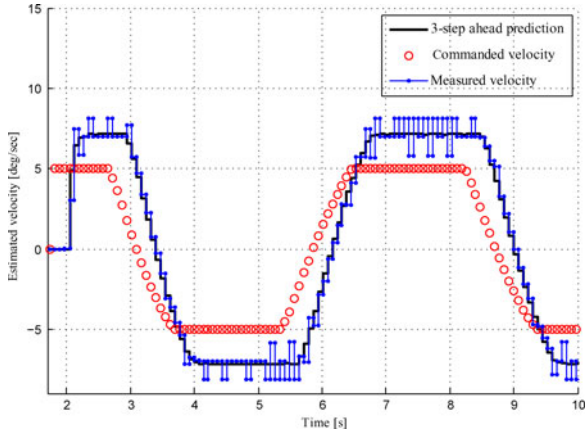

Fig. 4. Input/output joint velocity data from the KUKA-KR16 industrial manipulator. It is seen that a first-order model accurately describes the joint's velocity dynamics.

VII. Experiments

In this section, experimental results performed on a real industrial manipulator are presented. The verification of the proposed model (1) is first considered, followed by output feedback experiments with varying gains. Standard six-axes industrial manipulators (Kuka KR-16) were used in the experiments. Joint angles used in the output feedback scheme are measured from joint encoders using the Robot Sensor Interface (RSI). The RSI is limited to accept only velocity commands for motion control. Using the joint measurements for feedback control as is done here effectively emulates sensor-based feedback schemes which result from using position-based sensors such as cameras, laser sensors, or structured light sensors. The controller was implemented in MATLAB (2012a), and TCP/IP is used for the communication between MATLAB and the RSI. The sampling period is fixed at $T = 75$ ms. For more details regarding the experimental setup see [22].

A. Model verification

The model identification and verification for the KUKA-KR16 manipulator is presented in this section. Using sinusoidal velocity references for all joints simultaneously, an identification dataset was generated consisting of several thousands samples. By using least-squares identification, a was identified to be $0.329 \pm 2e - 4$ for each joint. The input parameter b was identified as 0.975 ± 0.0015 for each joint. The input to output time delay was identified as 3 samples, i.e., $d = 2$. The small variance of the model parameters as identified individually for the different joints show that a homogeneous model, as is considered here, is an accurate assumption. For the model verification, the periodic input velocity seen in Fig. 4 was commanded to each joint simultaneously. Fig. 4 shows also a three-step ahead prediction for the joint velocity using the identified model, which accurately predicts joint motions.

B. Sensor-based control experiments

In this section, we outline several output feedback experiments performed with different feedback gains. A picture of the laboratory setup is seen in Fig. 9. The camera-type task which is considered is to align the end effectors wrist axis toward a given point in space $\boldsymbol{p}$, which produces a task function in $\mathbb{R}^2$ [23]. This task produces four redundant degrees of freedom (DOF) for the 6-DOF manipulator which is used.

1) Task Kinematics: In this section, we shortly review the chosen task kinematics, and verify that they fulfill Assumptions 1–3. Let the

rotation matrix $\mathbf{R}$ describe the orientation of the end effector with the position $\boldsymbol{x}(\boldsymbol{q}_k)$, the considered task function $\boldsymbol{e}(\boldsymbol{q}_k)$ is given by

$$\boldsymbol{e}(\boldsymbol{q}) = \begin{bmatrix} \dfrac{y_1}{y_3+1} & \dfrac{y_2}{y_3+1} \end{bmatrix}^T \tag{38}$$

where the unit vector $\boldsymbol{y} = [y_1, y_2, y_3]^T$ is given by

$$\boldsymbol{y}(\boldsymbol{q}_k) = \mathbf{R}^{\mathbf{T}}(\boldsymbol{q}_{\mathbf{k}})(\boldsymbol{p} - \boldsymbol{x}_k)/\|\boldsymbol{p} - \boldsymbol{x}_k\| \in \mathbb{R}^3. \tag{39}$$

To verify that this task fulfills Assumptions 1–3, we compute the first and second partial derivatives of $\boldsymbol{e}$ with respect to joint angles q_i. The task Jacobian $\mathbf{J}$, as computed in [23], is given by

$$\mathbf{J} = \frac{\partial \boldsymbol{e}}{\partial \boldsymbol{y}} \mathbf{D} \mathbf{J}_m \tag{40}$$

where

$$\frac{\partial \mathbf{e}}{\partial \mathbf{y}} = 2 \begin{bmatrix} 1/(y_3+1) & 0 & -y_1/(y_3+1)^2 \\ 0 & 1/(y_3+1) & -y_2/(y_3+1)^2 \end{bmatrix} \tag{41}$$

$$\mathbf{D} = \begin{bmatrix} \frac{1}{\|\mathbf{p}-\mathbf{x}\|}\mathbf{S}^2(\mathbf{y})\mathbf{R}^T & \mathbf{S}(\mathbf{y})\mathbf{R}^T \end{bmatrix} \tag{42}$$

and $\mathbf{J}_m$ refers to the manipulator Jacobian pertaining to the robot specific kinematics, and $S(y)$ is the skew-symmetric operator representing the vector product. We choose the joint space region $\mathcal{Q}$ as

$$\mathcal{Q} = \mathbf{q} \in \mathbf{R}^n \text{ such that } \begin{cases} y_3(\mathbf{q}) > -1 + \epsilon_1 \\ \det(\mathbf{J}_m \mathbf{J}_m^T) > \epsilon_2 \\ \|\mathbf{p} - \mathbf{x}\| > \epsilon_3 \end{cases} \tag{43}$$

for some arbitrarily small positive numbers ϵ_i. The disallowed configurations, i.e., $y_3(\boldsymbol{q}) = -1$, correspond to an end-effector orientation which is misaligned by 180°. Moreover, we assume that the manipulator Jacobian $\mathbf{J}_m$ is nonsingular on $\mathcal{Q}$, and that the camera target is not the same as the end-effector position. We verify that Assumption 1 is fulfilled by computing the following bound of its spectral norm

$$\left\| \frac{\partial \boldsymbol{e}}{\partial \boldsymbol{y}} \right\| < \frac{2}{\epsilon_1}, \quad \|D\| = \sqrt{1 + \|\boldsymbol{p} - \boldsymbol{x}\|^{-2}}. \tag{44}$$

It follows from (40) that $\|\mathbf{J}\| < \frac{2\epsilon_2}{\epsilon_1}\sqrt{1 + \|\boldsymbol{p} - \boldsymbol{x}\|^{-2}} = \delta$. The details of the computations are omitted for clarity of exposition, but are easily computed by the definition of the spectral norm. Assumption 2 is valid since $\frac{\partial \boldsymbol{e}}{\partial \boldsymbol{y}}$ and $\mathbf{D}$ are nonsingular for all $\boldsymbol{q}$, such that their matrix product with $\mathbf{J}_m$ also is nonsingular. Assumption 3, imposes norm-boundedness of the second-order partial derivatives of $\boldsymbol{e}$ with respect to $\boldsymbol{q}$, which we may compute individually for each matrix by the chain rule. The partial derivatives of $\frac{\partial}{\partial \boldsymbol{q}_i}\mathbf{J}_m$ are bounded for a manipulator with rotational joints, which follows from the fact that the elements of the manipulator Jacobian is composed of trigonometric functions of $\boldsymbol{q}$. The only other terms that may become unbounded are the inverse $(1 + y_3)^{-1}$, which appear in the elements of $\frac{\partial^2 \boldsymbol{e}_j}{\partial \boldsymbol{q}_i}$, which is upper bounded on $\mathcal{Q}$ by construction. The partial derivatives of the matrix $\mathbf{D}$, is in part composed by $\frac{\partial \boldsymbol{y}}{\partial \boldsymbol{q}} = \mathbf{D}\mathbf{J}_m$, which is bounded by Assumption 1. The rest of the terms contain elements of the manipulator Jacobian, and their derivatives, which are bounded. It is hence verified that Assumptions 1–3 are true for the task (38) on $\mathcal{Q}$.

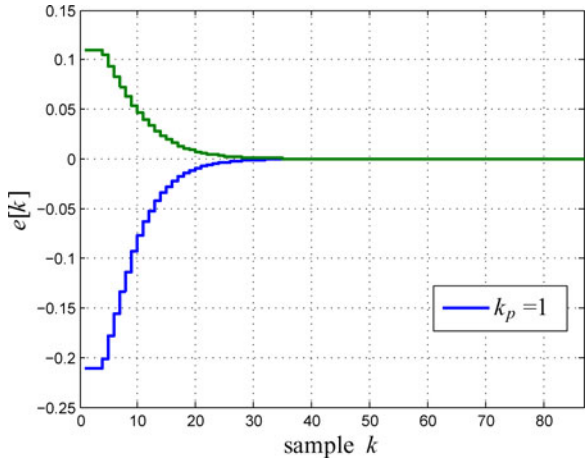

Fig. 5. Closed loop response for a small gain showing convergence to the origin for $\boldsymbol{e} = [e_1, e_2]^T$.

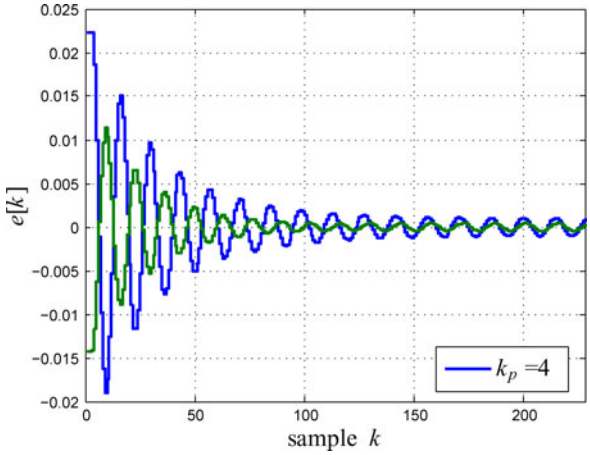

Fig. 6. Closed loop response for a gain on the stability threshold showing standing oscillations.

2) Experimental Results: Figs. 5–8 report the task function e_k for increasing feedback gains k_p. For low gains, exponential-like decay of the error is observed, while oscillations and divergence appears as the gain is increased past the stability threshold. This behavior, which is analogous to linear feedback systems responses, is what is expected from the theoretical small-gain local stability derived in Section V.

The stability threshold, which corresponds to standing oscillations seen in Fig. 6, was experimentally determined to be about $k_p = 4$ for the given initial condition.

The theoretical maximal gain, which is determined by considering the eigenvalues of $\mathbf{A}_{ee}(k_p)$ for the identified parameters, was calculated as $k_p = 5.435$. The theoretical result, while being slightly higher than the experimentally determined one, is reasonably close. The main source of error in the gain estimate is due to the simplicity of the model. Unmodeled effects include second-order dynamics, heterogeneous dynamics, and nonconstant signal delay. For instance, a delay estimate that is too low will result in a too high feedback gain threshold. However, it is not known which of these have the highest effect on the gain estimate.

The maximum allowed feedback in the trajectory generation case is $k_{p_{\max}} = 2/T = 28.5$ [19], which is higher. This is expected since in this case no sensory feedback is used, which remove the negative effects due to delay but is limited to open-loop control.

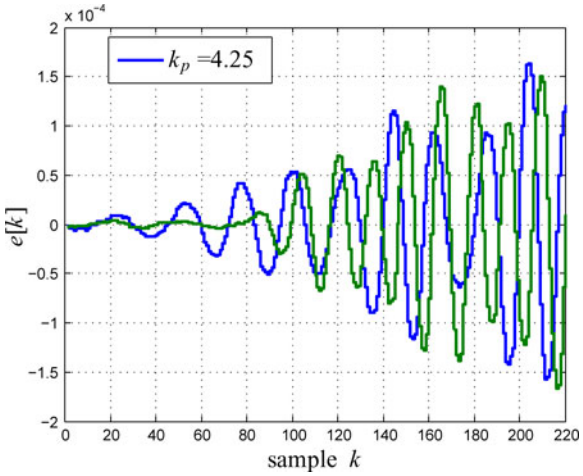

Fig. 7. Closed loop response for higher gains showing divergence.

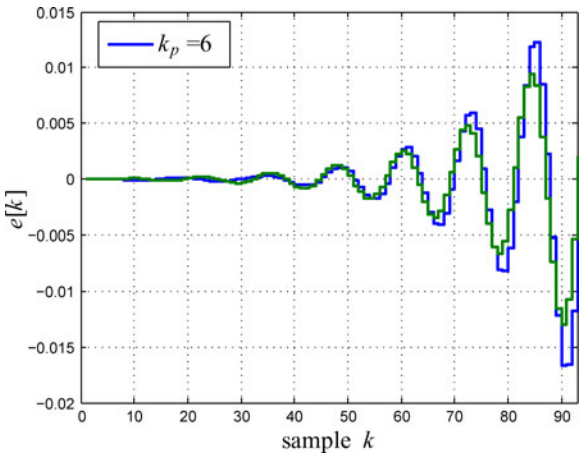

Fig. 8. Closed loop response for higher gains showing divergence from a very small initial error.

Fig. 9. KUKA KR16 industrial robot used in the experiments.

VIII. Conclusion and Further Work

This paper showed that the RMRC used for outer-loop kinematic control with a linearly stable inner loop, produces a locally asymptotically stable closed-loop system in the presence of delays. The result is applicable to systems with both minimum and nonminimum phase dynamics in the inner loop. A tight upper bound for the outer-loop feedback gain was derived for small delays and a small gain result was derived for arbitrary high delays. This result extends the knowledge of the stability of sensor-based feedback control schemes, e.g., visual servoing control.

In order to generalize the results future work will address heterogeneous inner-loop dynamics, as opposed to the homogeneous case considered here. This extension would be applicable to, for instance, coordinated control of nonidentical robots. Some preliminary results for heterogeneous dynamics may be found in [24]. The relevance of these results are currently limited as no delays are considered.

Stability results for the case where the damped pseudoinverse is used to increase the robustness to singularities is also an interesting extension that should be investigated in future work.

Appendix
Proof Of Proposition 1

The proof of Proposition 1 is presented here, which is based on Jury's test. Consider the characteristic equation $\det(\mathbf{A}_{ee} - \mathbf{I}\lambda) = 0$

$$\left(\lambda^{d+1} - (1+a)\lambda^d + a\lambda^{d-1} + k_p T b\right)^m = 0. \tag{45}$$

We define $g = k_p T b > 0$ for simplicity and note that it is sufficient to show that the roots of

$$f(\lambda) = \lambda^{d+1} - (1+a)\lambda^d + a\lambda^{d-1} + g \tag{46}$$

are strictly inside the unit circle. For an nth order polynomial, Jury's test generates $n+1$ functions $p_i(a,g)$ (see [25]). If $p_i(a,g)$ are all positive, then the solutions to (46) satisfy $|\lambda_j| < 1$. Since the functions p_i become quite complicated as the order i increases, we will limit our calculation to the first two coefficients of the Taylor series of $p_i(g)$ around $g = 0$, which are significantly simpler. The zeroth-order terms are calculated as

$$\mathbf{p}(g=0) = [\,1 \quad 1 \quad \ldots \quad 1-a^2 \quad 0\,]. \tag{47}$$

These are easily calculated by generating the Jury table for $f(\lambda)|_{g=0}$. The table for the first-order coefficients with the elements $\partial p_i = \frac{\partial p_i}{\partial g}\big|_{g=0}$ are calculated as

$$\partial p_{i<n} = 0 \tag{48}$$

$$\partial p_n = -2a(a^{d-1} + a^{d-2} \ldots + a + 1) \tag{49}$$

$$\partial p_{n+1} = 2(1-a). \tag{50}$$

The detailed generation of $\boldsymbol{p}, \partial\boldsymbol{p}$ is omitted due to the lack of space, but is easy to replicate and both Jury tables exhibit quite simple sparse structures. To see that (47)–(48) implies that $p_i > 0$, generate the new table

$$\mathbf{p}' = \left[p_1 \;\; p_1 p_2 \;\; p_1 p_2 p_3 \;\; \ldots \;\; \prod_{i=1}^{n+1} p_i\right]. \tag{51}$$

Clearly, $p_i > 0 \iff p_i' > 0$ for all i. To see that $p_i > 0 \Leftarrow p_i' > 0$, first note that $p_1' = p_1 > 0$, then divide the rest of the elements $p_{i>1}'$ by p_1, and note that the second element p_2'/p_1 is now equal to $p_2 > 0$. Iterate until the table $\boldsymbol{p}$ is replicated. The implication from left to right is trivial. The crucial property of the coefficients p_i' is that they are polynomials in both g and a, in contrast with p_i which are rational functions of g, a. To verify this fact, we assume that the elements of the jth row in the Jury-table $\mathbf{W}_j^T$ is a polynomial in (a,g), i.e.,

$$\mathbf{W}_j^T = [\,p_j \quad w_{n-1} \quad \ldots \quad w_0\,]$$

$$\mathbf{W}_{j+1}^T = \left[\,p_j - w_0\frac{w_0}{p_j} \quad w_{n-1} - w_1\frac{w_0}{p_j} \quad \ldots \quad 0\,\right].$$

Here, the first element of $\mathbf{W}_{j+1}^T$ is the next coefficient $p_{j+1} = p_j - w_0 \frac{w_0}{p_j}$. Clearly, $p_{j+1}^{'} = p_{j+1}p_j = p_j^2 - w_0^2$ is a polynomial in both a and g. To see that the all $p_i^{'}$ are all polynomials in a and g, it suffices to note that the first row of $\mathbf{W}_1^T$ contains the coefficients of $f(\lambda)$, which are first-order polynomials in a, g, and use induction.

We can now see that for some g small enough, $p_i^{'} > 0$. For the first $n-1$ elements p_i, we have that $p_i^{'}(g=0) = 1, \partial p_i^{'}(g=0) = 0$, such that

$$p_j^{'}(g) = 1 + g\sum_{l=1}^{N_j} \alpha_l(a) g^l, \quad \forall j \in [1, n-1] \tag{52}$$

where $\alpha_l(a)$ are now polynomials in only a, and N_j is a positive integer. It is seen from (52) that there exist a small enough g such that $p_j^{'} > 0$. For $p_n^{'}$, we have

$$p_n^{'}(g) = (1-a^2) + \sum_{l=1}^{N_n} \beta_l(a) g^l \tag{53}$$

and again this is positive for some g small enough. Finally, we have

$$p_{n+1}^{'}(g) = 2g(1-a) + g\sum_{l=1}^{N_{n+1}} \epsilon_l(a) g^l \tag{54}$$

dividing $p_{n+1}^{'}$ by g shows again that for some g small enough we have $p_{n+1}^{'}/g > 0$ since $(1-a) > 0$. In summary, there exist some g small enough such that $p_{n+1}^{'} > 0$, which implies that $p_i > 0$, and hence $|\lambda_i| < 1$ by Jury's test. This completes the proof.

REFERENCES

[1] B. Siciliano and O. Khatib, *Springer Handbook of Robotics*. New York, NY, USA: Springer-Verlag, 2008.

[2] K. Nilsson, "Industrial robot programming" Ph.D. dissertation, Dept. Automatic Control, Lund Inst. Technol., Lund, Sweden, 1996.

[3] P. Corke, "The unimation puma servo system," MTM-226, CSIRO Div. Manuf. Technol., Australia, Tech. Rep., 1994.

[4] T. I. Fossen, *Handbook of Marine Craft Hydrodynamics and Motion Control*. New York, NY, USA: Wiley, 2011.

[5] N. Vuong, V. Ang, T. M. Lim, and S. Y. Lim, "Multi-rate operational space control of compliant motion in robotic manipulators," in *Proc. IEEE Int. Conf. Syst., Man Cybern.*, 2009, pp. 3175–3180.

[6] D. Whitney, "Resolved motion rate control of manipulators and human prostheses," *IEEE Trans. Man-Mach. Syst.*, vol. MMS-10, no. 2, pp. 47–53, Jun. 1969.

[7] A. Balestrino, G. De Maria, and L. Sciavicco, "Robust control of robotic manipulators," in *Proc. 9th IFAC World Congr.*, Jul. 1984, vol. 6, pp. 80–85.

[8] S. Hutchinson, G. Hager, and P. Corke, "A tutorial on visual servo control," *IEEE Trans. Robot. Autom.*, vol. 12, no. 5, pp. 651–670, Oct. 1996.

[9] B. Siciliano, "Kinematic control of redundant robot manipulators: A tutorial," *J. Intell. Robot. Syst.*, vol. 3, no. 3, pp. 201–212, 1990.

[10] A. Marino, L. E. Parker, G. Antonelli, and F. Caccavale, "A decentralized architecture for multi-robot systems based on the null-space-behavioral control with application to multi-robot border patrolling," *J. Intell. Robot. Syst.*, vol. 71, pp. 1–22, 2012.

[11] J. Moreno and R. Kelly, "Hierarchical velocity field control for robot manipulators," in *Proc. IEEE Int. Conf. Robot. Autom.*, Sep. 2003, vol. 3, pp. 4374–4379.

[12] J. Lee, N. Mansard, and J. Park, "Intermediate desired value approach for task transition of robots in kinematic control," *IEEE Trans. Robot.*, vol. 28, no. 6, pp. 1260–1277, Dec. 2012.

[13] P. Falco, C. Natale, and R. Dillmann, "Ensuring kinetostatic consistency in observation of human manipulation," *Robot. Auton. Syst.*, vol. 61, pp. 545–553, 2013.

[14] T. Kroger and F. Wahl, "Online trajectory generation: Basic concepts for instantaneous reactions to unforeseen events," *IEEE Trans. Robot.*, vol. 26, no. 1, pp. 94–111, 2010.

[15] M. Aicardi, A. Caiti, G. Cannata, and G. Casalino, "Stability and robustness analysis of a two layered hierarchical architecture for the closed loop control of robots in the operational space," in *Proc. IEEE Int. Conf. Robot. Autom.*, May 1995, vol. 3, pp. 2771–2778.

[16] C. Natale, R. Koeppe, and G. Hirzinger, "A systematic design procedure of force controllers for industrial robots," *IEEE/ASME Trans. Mechatronics*, vol. 5, no. 2, pp. 122–131, Jun. 2000.

[17] R. Kelly and J. Moreno, "Manipulator motion control in operational space using joint velocity inner loops," *Automatica*, vol. 41, no. 8, pp. 1423–1432, 2005.

[18] K. Camarillo, R. Campa, V. Santibáñez, and J. Moreno-Valenzuela, "Stability analysis of the operational space control for industrial robots using their own joint velocity pi controllers," *Robotica*, vol. 26, no. 6, pp. 729–738, 2008.

[19] P. Falco and C. Natale, "On the stability of closed-loop inverse kinematics algorithms for redundant robots," *IEEE Trans. Robot.*, vol. 27, no. 4, pp. 780–784, Aug. 2011.

[20] E. Conkur and R. Buckingham, "Clarifying the definition of redundancy as used in robotics," *Robotica*, vol. 15, no. 5, pp. 583–586, 1997.

[21] J. Hurt, "Some stability theorems for ordinary difference equations," *SIAM J. Numer. Anal.*, vol. 4, pp. 582–596, 1967.

[22] M. Bjerkeng, A. Transeth, K. Pettersen, E. Kyrkjebo, and S. Fjerdingen, "Active camera control with obstacle avoidance for remote operations with industrial manipulators: Implementation and experimental results," in *Proc. IEEE/RSJ Int. Conf. Intell. Robots Syst.*, 2011, pp. 247–254.

[23] M. Bjerkeng, K. Y. Pettersen, and E. Kyrkjebo, "Stereographic projection for industrial manipulator tasks: Theory and experiments," in *Proc. IEEE/RSJ Int. Conf. Intell. Robots Syst.*, Sep. 2011, pp. 4676–4683.

[24] M. Bjerkeng, P. Falco, C. Natale, and K. Pettersen, "Discrete-time stability analysis of a control architecture for heterogeneous robotic systems," in *Proc. IEEE/RSJ. Int. Conf. Intell. Robots Syst.*, 2013, pp. 4778–4783.

[25] M. Benidir, "On the root distribution of general polynomials with respect to the unit circle," *Signal Process.*, vol. 53, no. 1, pp. 75–82, 1996.

Torso Inclination Enables Faster Walking in a Planar Biped Robot With Passive Ankles

Tao Geng

***Abstract*—There is a category of biped robots that are equipped with unactuated or passive ankles. We call them passive ankle walkers (PAWs). Because the unactuated ankle cannot provide the push-off at the end of stance phase as human ankles do, fast walking in PAWs is more challenging. In this paper, in order to realize fast walking in PAWs, we propose a simple strategy—torso inclination. To test this strategy, we studied a PAW model with simulation and prototype experiments. The simulation has shown how the torso inclination affects the walking speed and the energy efficiency of the PAW. Considering the "reality gap" problem of simulation, we have also experimentally tested this strategy with a real robot. By analyzing both the simulated model and the experimental results of the real robot, we identified the mechanism that accounts for fast walking in torso-inclined PAW.**

***Index Terms*—Biped robots, legged locomotion, limit cycle walker.**

I. INTRODUCTION

In this section, we first review some typical planar biped robots that have been designed for fast walking. Then, we explain why fast walking is challenging in passive ankle walkers (PAWs). Finally, we propose our strategy for fast walking in PAWs, and highlight the contributions of this study.

Manuscript received May 29, 2013; revised October 25, 2013; accepted December 27, 2013. Date of publication January 17, 2014; date of current version June 3, 2014. This paper was recommended for publication by Associate Editor Y. Choi and Editor A. Kheddar upon evaluation of the reviewers' comments.

The author is with the Department of Electronic Engineering, University of Surrey, Guildford, Surrey GU2 7XH, U.K. (e-mail: runbot05@gmail.com).

Color versions of one or more of the figures in this paper are available online at http://ieeexplore.ieee.org.

Digital Object Identifier 10.1109/TRO.2014.2298058